



A prediction model of mass transfer through an electro dialysis cell

Azadeh Ghorbani^{a,*}, Abbas Ghassemi^{a,b}, Paul K. Andersen^{a,b}, Reza Foudazi^b

^a*Institute for Energy and the Environment (IEE/WERC), New Mexico State University, Las Cruces, NM, USA, Tel. +1 575 646 7820; email: azadeh12@nmsu.edu (A. Ghorbani), Tel. +1 575 646 5474; email: aghassem@nmsu.edu (A. Ghassemi), Tel. +1 575 646 8153; email: pka@nmsu.edu (P.K. Andersen)*

^b*Department of Chemical and Materials Engineering, New Mexico State University, Las Cruces, NM, USA, Tel. +1 575 646 2073; email: rfoudazi@nmsu.edu (R. Foudazi)*

Received 13 May 2015; Accepted 12 November 2015

ABSTRACT

The purpose of this work is to develop a mass transfer model that incorporates all relevant factors—migration, diffusion, and convection—to predict ion transfer in electro dialysis cells more completely than conventional models, which neglect convection. As a demonstration of this approach, the study develops a three-dimensional model that incorporates the factor of convection to predict NaCl mass transport through a rectangular electro dialysis cell. The equations used in the model—the complete Navier–Stokes, continuity, and steady-state Nernst–Planck equations—are solved by the finite difference numerical method in the particular control volumes. The equations in the dilute chamber are numerically solved using techniques from computational fluid dynamics (CFD). In order to evaluate the reliability and accuracy of the model, the results are compared with theory as calculated by the Nernst–Planck equation. We discovered that the developed model is capable of predicting the velocity distribution, separation percent, ion concentration distribution, and electrolyte potential in the chamber, with results that closely align with the theory. Additionally, by considering all three contributions, the developed model could predict a detailed distribution of concentration and potential drop in both the x - and y -directions.

Keywords: Electro dialysis; Modeling; CFD; Convection

1. Introduction

Water is one of the most important natural resources in the world, and without it life cannot exist. The presence of a safe and reliable source of water is essential. Fresh water, however, is scarce—the U.S. Geological Survey reports that only 0.8% of Earth's water is considered to be fresh [1–4]. Therefore, it is essential to find alternative water sources.

For producing drinking water from nontraditional sources, one of the most promising methods is desalination, the process of turning brackish or sea water into fresh water. All natural waters contain dissolved salts at different concentrations, and water with elevated salt levels is available almost everywhere around the world. Recent technological advancements suggest that the wide-scale desalination of these salt water sources could mitigate the impact of freshwater scarcity [3]. To reduce the salt content of saline water, several processes are available, including distillation, ion-exchange (IE), reverse osmosis (RO), nanofiltration

*Corresponding author.

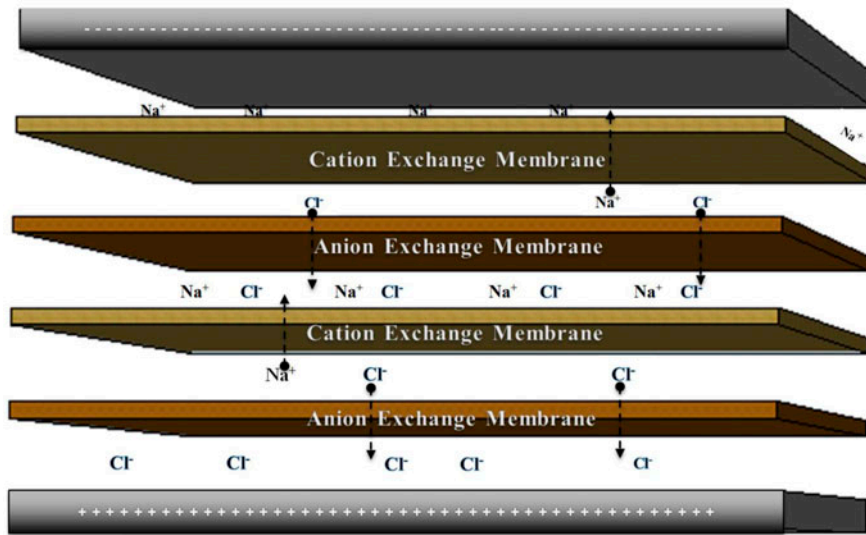


Fig. 1. Schematic of ED System.

(NF), membrane distillation (MD), electrodialysis (ED), and neutralization dialysis (ND) [2].

The present research focuses on ED, a membrane separation process in which IE membranes are employed to separate ions from an aqueous solution under the influence of an electrical driving force. This technique has been applied for over 50 years in the desalination of natural water and represents one of the most important desalination methods [1–9]. A schematic view of an ED cell is outlined in Fig. 1.

As can be seen from Fig. 1, an ED cell consists of a series of anion- and cation-exchange membranes (CEMs) arranged in an alternating pattern between an anode and a cathode. When DC potential is applied to the system, cations move toward the cathode, passing the CEMs but becoming trapped by the anion-exchange membranes (AEM), while anions move toward the anode, passing the AEMs but becoming trapped by the CEMs. This pattern of ion movement

creates two alternating types of chambers between membranes: a dilute chamber, in which ions have largely been removed, and a concentrate chamber, where trapped ions are amassed.

In the ED process, the ion transport model is important since it can lay out the entire picture of electron transport in the ED cell. This makes it possible to describe the ion transport and predict the performance of the ED system. To describe mass transport phenomena in ED, the Nernst–Planck equation can be applied [5]:

$$J_i = -D\nabla c_i - \frac{Dz_iFc_i}{RT} \nabla\phi - vc_i \tag{1}$$

The first term in this equation represents diffusion due to a concentration gradient, the second term is migration due to an electrical potential gradient, and the third term is convection due to a pressure gradient.

Many theoretical studies based on the Nernst–Planck equation have been carried out to investigate transfer processes through IE membranes [10–31]. For the sake of simplicity, these studies have neglected the convection term. For example, Kim et al. developed a mathematical model to simulate the steady-state transport of three ions in an ED cell on the basis of diffusion and migration. However, the research team ignored the effect of convection on the Nernst–Planck equation [32]. Other studies have developed a semi-empirical model that is based on Nernst–Planck and that has been tested for

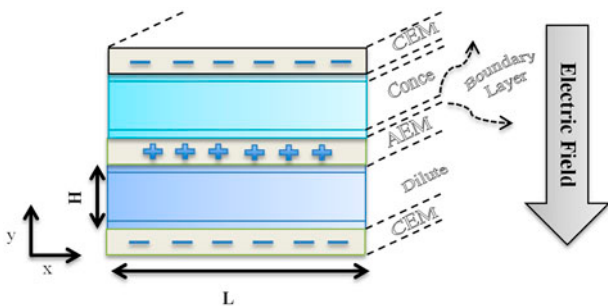


Fig. 2. Model geometry.

Table 1
Ionic concentration and potential drop in the boundary layer near CEM

$$y: c_2 = \frac{z_1 [k_1(y - \delta_1) + c_1^b + c_2^b]}{z_1 - z_2} \quad (11)$$

$$x: c_2 = \frac{z_1 [k_1 x + c_2^b]}{k_3 + z_1 - z_2} \quad (12)$$

$$y: \Delta\theta = \theta_y - \theta_{y=\delta_1} = \frac{-RT}{z_1 F} \left(\ln \frac{c_1}{c_1^b} \right) \quad (13)$$

$$x: \Delta\theta = \theta_x - \theta_{x=0} = \frac{-RT}{z_1 F} \left(\ln \frac{c_1}{c_1^b} + \frac{(y^2 - \frac{H^2}{2})\Delta p}{2\mu L D_1} \right) \quad (14)$$

$$k_1 = \frac{I}{z_2 D_2 F} \quad (15)$$

$$k_3 = \left(\frac{z_1}{D_2} - \frac{z_2}{D_1} \right) \left[\frac{(y^2 - \frac{H^2}{2})\Delta p}{2\mu} \right] \quad (16)$$

Table 2
Ionic concentration and potential drop in the boundary layer near AEM

$$y: c_1 = \frac{z_2 [k_2(y - \delta_2) + c_1^b + c_2^b]}{z_2 - z_1} \quad (17)$$

$$x: c_1 = \frac{z_2 [k_2 x + c_1^b]}{k_4 + z_2 - z_1} \quad (18)$$

$$y: \Delta\theta = \theta_y - \theta_{y=\delta_2} = \frac{-RT}{z_2 F} \left(\ln \frac{c_2}{c_2^b} \right) \quad (19)$$

$$x: \Delta\theta = \theta_x - \theta_{x=0} = \frac{-RT}{z_2 F} \left(\ln \frac{c_2}{c_2^b} + \frac{(y^2 - \frac{H^2}{2})\Delta p}{2\mu L D_2} \right) \quad (20)$$

$$k_2 = \frac{I}{z_1 D_1 F} \quad (21)$$

$$k_4 = \left(\frac{z_2}{D_1} - \frac{z_1}{D_2} \right) \left[\frac{(y^2 - \frac{H^2}{2})\Delta p}{2\mu} \right] \quad (22)$$

consistency against experimental data from various hydrodynamic conditions [10,14,30]. Existing models of the transfer process have not yet incorporated the convection term, leaving the models incomplete.

Table 3
Ionic concentration and potential drop in the membrane

$$\text{Ionic transport in a CEM} \quad \Delta\theta = \frac{RT}{FQ_{CEM}} \left[\Delta c_1 - \frac{I}{z_1 F D_1^m} (\Delta y) \right] \quad (26)$$

$$\text{Ionic transport in an AEM} \quad \Delta\theta = \frac{RT}{FQ_{AEM}} \left[\Delta c_1 - \frac{I}{z_2 F D_2^m} (\Delta y) \right] \quad (27)$$

Table 4
Dimensionless governing equations

$$U_x \frac{\partial U_x}{\partial X} + U_y \frac{\partial U_y}{\partial Y} = \frac{1}{Re} \left(\frac{\partial^2 U_x}{\partial X^2} + \frac{\partial^2 U_x}{\partial Y^2} \right) - \frac{\partial P}{\partial X} \quad \text{Momentum transport} \quad (28)$$

$$U_x \frac{\partial U_y}{\partial X} + U_y \frac{\partial U_y}{\partial Y} = \frac{1}{Re} \left(\frac{\partial^2 U_y}{\partial X^2} + \frac{\partial^2 U_y}{\partial Y^2} \right) - \frac{\partial P}{\partial Y} + f_y \quad (29)$$

$$\frac{\partial U_x}{\partial X} + \frac{\partial U_y}{\partial Y} = 0 \quad \text{Continuity equation} \quad (29)$$

$$U_x \frac{\partial C}{\partial X} + U_y \frac{\partial C}{\partial Y} = \frac{1}{Pe} \left(\frac{\partial^2 C}{\partial X^2} + \frac{\partial^2 C}{\partial Y^2} \right) - \frac{\partial C}{\partial t} \quad \text{Mass transport} \quad (30)$$

$$f_y = \frac{\varepsilon E R T}{|z| F H \rho_{0y}} \frac{\partial^2 \theta}{\partial Y^2} \quad \text{Body force} \quad (31)$$

$$J = -\frac{\partial C}{\partial Y} - c \frac{\partial \theta}{\partial Y} - Pe(\text{UC}) \quad \text{Nernst-Planck} \quad (32)$$

$$\Delta\theta = \ln \left(\frac{C_{y=0,H}}{C} \right) \quad \text{Donnan potential drop} \quad (33)$$

The purpose of this study is to develop a complete model that considers all three contributions—diffusion, migration, and the previously ignored term of convection—that play a role in ion transfer in ED cells. In order to provide a complete model that estimates the effects of different parameters on ion separation, the Navier–Stokes, continuity, and Nernst–Planck equations in two dimensions are used for the dilute chamber. To solve the set of equations, the finite difference method is employed. Current density is considered to be constant in each run.

2. Model development

A mass transfer model is developed to simulate ion transport for NaCl in an ED cell pair. The model is based on steady-state, isothermal, and two-dimensional mass transfer.

The model domain includes a two-dimensional cell pair where current flows in the y -direction and water flows in the x -direction. Fig. 2 shows more details of the computational domain, including the channel geometry and the associated coordinate system. The control volume is composed of three ion-selective membranes (the top and bottom membranes are permeable only to cations, and the middle membrane is permeable only to anions), two compartments (a dilute compartment where the ion concentration will decrease, and a concentrate compartment where the ion concentration will increase), and four boundary layers.

Table 5
Equations used in modeling

$\frac{\partial^2 \phi}{\partial y^2} = \beta \zeta \sinh(\alpha \frac{\phi}{\zeta})$	Poisson–Boltzmann [34]	(34)
$\alpha = \frac{e z \zeta}{k_b T}$	[34]	(35)
$\beta = \frac{(\omega H)^2}{\alpha}$	[34]	(36)
$\omega = \frac{1}{\lambda} = \sqrt{\frac{8 \pi n_0 e^2 z^2}{D k_b T}}$	Debye–Huckel [34]	(37)

In the present study, two ion species are considered: sodium (Na⁺) and chloride (Cl⁻). The sodium ions in the feed solution are transported through the CEM and the chloride ions are transported through the AEM. Therefore, at the CEM, the chloride ion flux is zero; at the AEM, the sodium ion flux is zero. We assume electroneutrality in the system.

2.1. Theory of the model

Ionic transport in two directions (x and y) is described below, while in Kim et al. model the simulation was in one direction [32]. For transport along the flow path (the x-direction), the convection term is considered in each control volume, while the convection term in the y-direction is small enough to be neglected.

2.1.1. Ionic transport in bulk

It is assumed that the fluid bulk is completely mixed, eliminating the diffusion term. Consequently, the ionic flux equation (Eqs. (2) and (3)) can be written with migration and convection [32]. The current density (i) can be calculated using Faraday’s law as in Eq. (4):

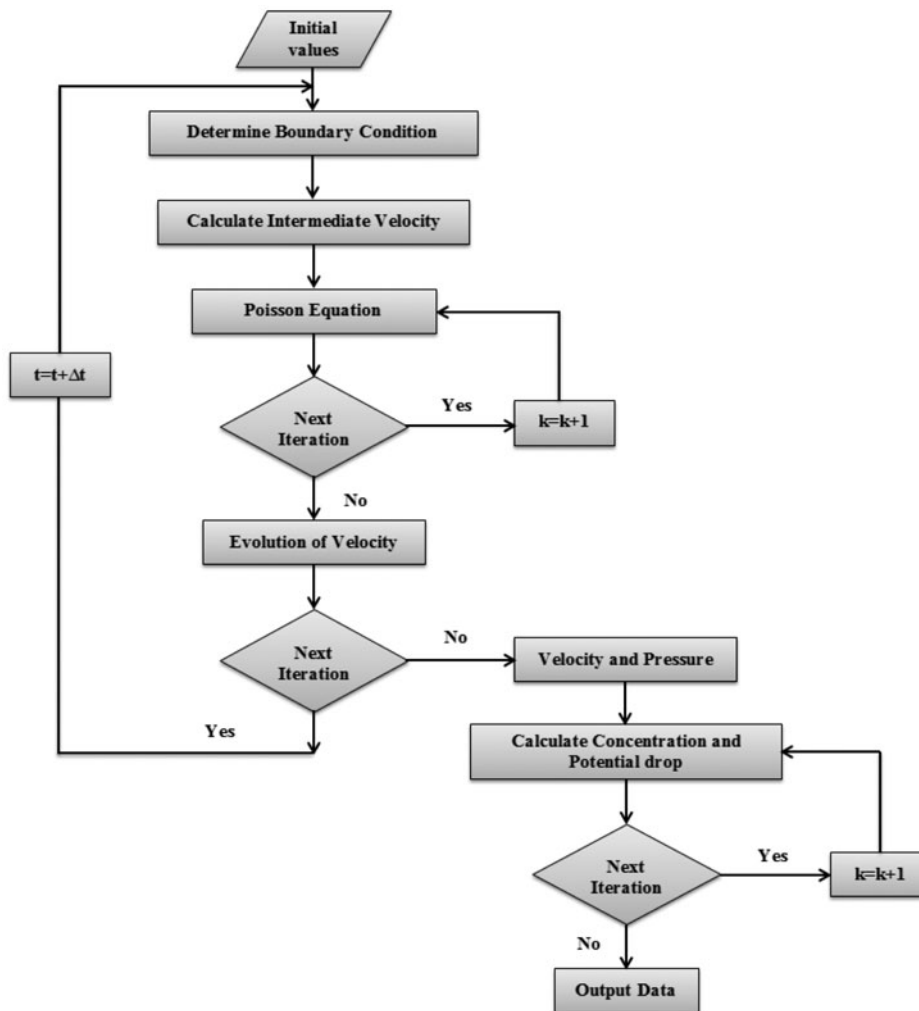


Fig. 3. Process modeling algorithm.

Table 6
Parameters of the mode

c_{in}	1,000 (ppm)	Initial feed concentration
D_{Na}	1.334×10^{-9} (m ² /s)	Diffusion coefficient for Na ⁺
D_{Cl}	2.032×10^{-9} (m ² /s)	Diffusion coefficient for Cl ⁻
D	80 (-)	Dielectric constant
d_a	0.6e-2 (m)	Anion-exchange membrane thickness
d_c	0.6e-2 (m)	Cation-exchange membrane thickness
E	15 (v)	Applied voltage
H	0.4e-3 (m)	Channel width
L	0.08 (m)	Channel length
i	50 (Amp/m ²)	Current density
Q	110 (ml/min)	Flow rate
Q_{CEM}	-2.1 (meq/gr)	Cation-exchange capacity
Q_{AEM}	2.63 (meq/gr)	Anion-exchange capacity
Re	50 (-)	Reynold number
T	298.15 (k)	Temperature
μ	8.98×10^{-4} (Pa s)	Water viscosity
ρ	1,000 (kg/m ³)	Water density
ζ	(-0.03–0.03) (v)	Zeta potential

$$x : j_i = -\frac{Dz_iFc_i}{RT} \frac{d\phi}{dx} - \frac{1}{2\mu} c_i \left(y^2 - \frac{H^2}{4} \right) \frac{dp}{dx} \quad (2)$$

$$y : j_i = -\frac{Dz_iFc_i}{RT} \frac{d\phi}{dy} \quad (3)$$

$$i = F \sum_i z_i j_i \quad (4)$$

Therefore, the potential drop can be written as follows:

$$x : \frac{d\phi}{dx} = -\frac{RTi}{D_{ij}z_i2F^2c_b} - \frac{RTA_1}{z_iFD_{ij}} \left(y^2 - \frac{H^2}{4} \right) \quad (5)$$

$$y : \frac{d\phi}{dy} = -\frac{RTi}{D_{ij}z_i2F^2c_b} \quad (6)$$

$$A_1 = \frac{\Delta p}{2\mu L} \quad (7)$$

For ionic species i (1 for cation and 2 for anion), j is the molar flux (mol/m²/s), z is the ionic charge, D is the diffusivity (m²/s), c is the molar concentration (mol/m³), T is the absolute temperature (K), ϕ is the potential (V), i is the current density (A/m²), F is the Faraday constant (96,485 C/mol), and R is the universal gas constant (8.314 J/mol/K).

2.1.2. Ionic transport in the boundary layer

In the boundary layer, all three contributing transport factors are present: diffusion, migration, and convection.

The Nernst–Planck equation, which considers convection from flow along the membrane, was employed in the steady-state mass balance equation, as in Eq. (8); and for transport toward the membrane, the convection term can be ignored as in Eq. (9). For a system consisting of a membrane and solutions, the condition described by Eq. (10) is called electroneutrality:

$$x : J_i = -D \frac{dc_i}{dx} - \frac{Dz_iFc_i}{RT} \frac{d\phi}{dx} - \frac{\left(y^2 - \frac{H^2}{2} \right) c_i}{2\mu} \frac{dp}{dx} \quad (8)$$

$$y : J_i = -D \frac{dc_i}{dy} - \frac{Dz_iFc_i}{RT} \frac{d\phi}{dy} \quad (9)$$

$$\sum_i z_i c_i = 0 \quad (10)$$

For a given transport number, the steady-state mass balance equation (Eqs. (8) and (9)) can be integrated and solved for the concentration and potential drop in the boundary layers near the CEM and AEM. For additional information, see Tables 1 and 2.

2.1.3. Ionic transport in membrane

Assuming a homogeneous distribution of ionic charges in the CEM and AEM, the steady-state mass balance equation is written with Eqs. (23) and (24) for the CEM and AEM, respectively [32].

The IE membrane is assumed to be occupied only by the species under consideration. Therefore, the ionic concentration is equivalent to the IE capacity (Q_{CEM} or Q_{AEM}), as in Eq. (25):

$$\frac{dc_1}{dy} + \frac{z_1 F}{RT} c_1 \frac{d\phi}{dy} = -\frac{I}{z_1 F D_1^m} \tag{23}$$

$$\frac{dc_2}{dy} + \frac{z_2 F}{RT} c_2 \frac{d\phi}{dy} = -\frac{I}{z_2 F D_2^m} \tag{24}$$

$$c = -\frac{Q_{CEM}}{z} \tag{25}$$

Table 3 shows the potential drop in the CEM and AEM.

Membrane-phase diffusivity, D^m , was approximated as one-tenth of the diffusivity in the infinitely dilute solution [33].

2.2. Model equations

Table 4 shows the conservation of momentum and mass equations that were used to model, in Cartesian coordinates, the movement of ions and water in the ED cell.

In these equations, U is the velocity vector, P is pressure, ϵ is dielectric constant, E is electric field, and ρ is density of fluid.

Additional equations used to develop the model are shown in Table 5, which contains Eqs. (34) through (37). The Poisson–Boltzmann equation (Eq. (34)) can be used to describe the electric potential distribution in the cell. In this equation, α is the ionic energy parameter and β is a variable. In Eq. (36), ω is the Debye–Huckel parameter, which is the inverse of Debye length (λ). In Eq. (37), e is the electron charge

(C), k_b is the Boltzmann constant (j/k), and n_0 is ion density (mol/m^3).

2.3. Boundary conditions

The boundary conditions at the boundaries between the membranes and the solution are described in Sections 2.3.1 and 2.3.2 [27].

2.3.1. Fluid boundary conditions

At the inlets of the channels, the fluid velocity is uniform and specified:

$$u_x(0, y) = u_i, \quad u_y(0, y) = 0$$

$$p(0, y) = p_{in}, \quad \frac{\partial p(L, y)}{\partial y} = 0$$

At the AEM and CEM, the no-slip boundary condition is applied for velocity. Consequently,

$$u_x(x, 0) = u_y(x, H) = 0$$

$$p(x, 0) = p(x, H) = 0.$$

2.3.2. Mass boundary conditions

At the inlets of the channels, the salt concentration is constant and specified:

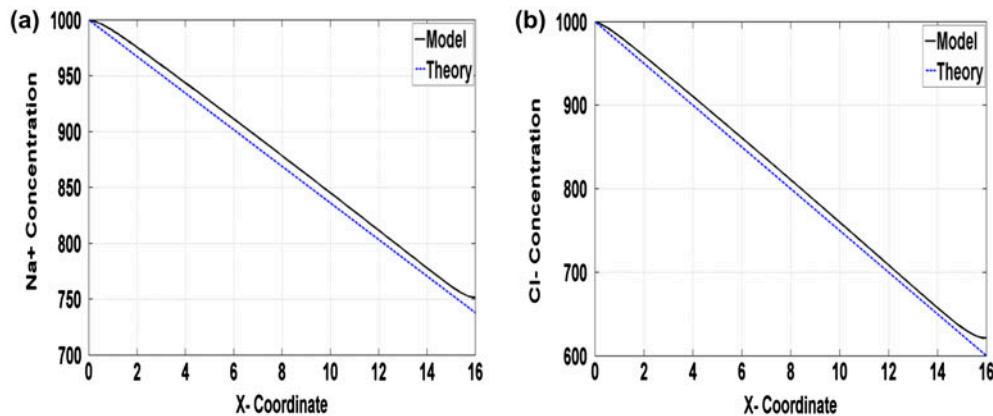


Fig. 4. Comparison between concentration profile in dilute chamber for (a) Na^+ and (b) Cl^- predicted by this model and the theory.

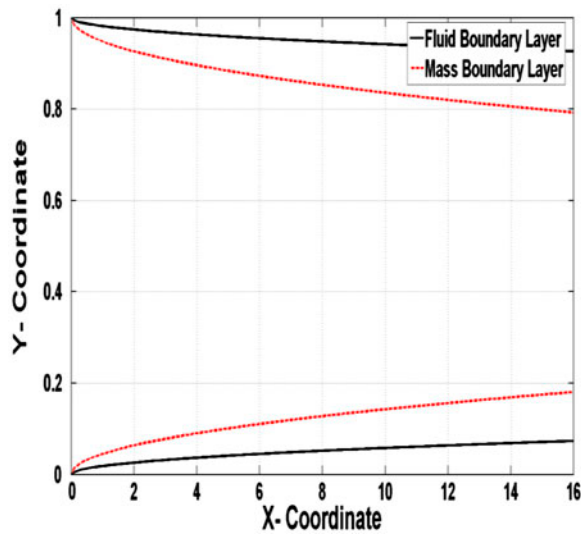


Fig. 5. Fluid and mass boundary layers thickness in dilute compartment ($Re = 50$).

$$c(0, y) = c_0 = c_{Na} = c_{Cl}$$

At the end of the channels, there is no diffusion flux; thus:

$$\frac{\partial c(L, y)}{\partial x} = 0$$

At the AEM there is only anion flux, while at the CEM there is only cation flux. These conditions can be written as follows:

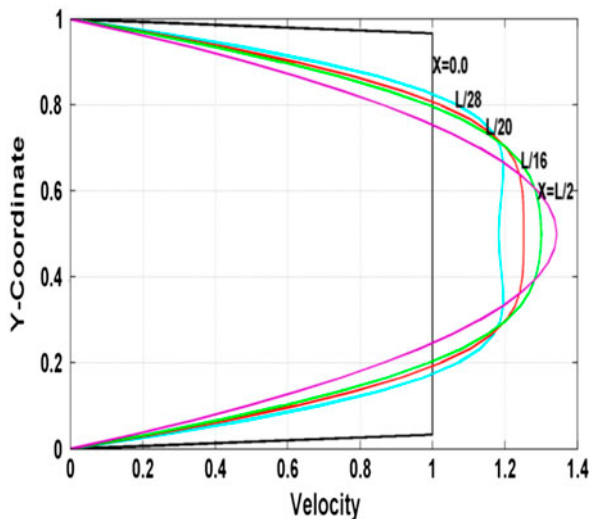


Fig. 6. Velocity distribution in dilute compartment along the Y-coordinate ($Re = 50$).

$$\frac{\partial c_{Na}(x, 0)}{\partial y} = \frac{i}{FD}$$

$$\frac{\partial c_{Cl}(x, H)}{\partial y} = \frac{i}{FD}$$

The model equations, including continuity, Navier–Stokes, and Nernst–Planck, were solved numerically, along with their appropriate bounding conditions, using MATLAB software.

2.4. Numerical procedure

In the implicit finite difference method for approximating the solutions to the continuity, Navier–Stokes, and Nernst–Planck equations, we have followed the sequence of steps shown in Fig. 3.

The process begins at “Initial Value” with the experimental identification of ED parameters, such as pressure, velocity, concentration, and membrane thickness, among others. After the identification of the system parameters, the boundary conditions are chosen, and then the intermediate velocity is calculated. Next, to determine pressure, the pressure Poisson equation is applied, and an iterative use of the finite difference method is employed to solve the equation approximately. So long as ε_1 (Eq. (38)) is larger than the predetermined error value, the iterations continue.

When ε_1 is smaller than the predetermined error value, the identified value for pressure is used in

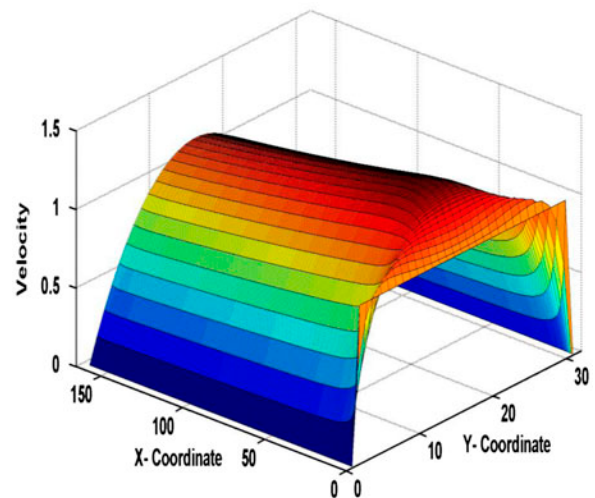


Fig. 7. Three-dimensional velocity profile in dilute compartment ($Re = 50$).

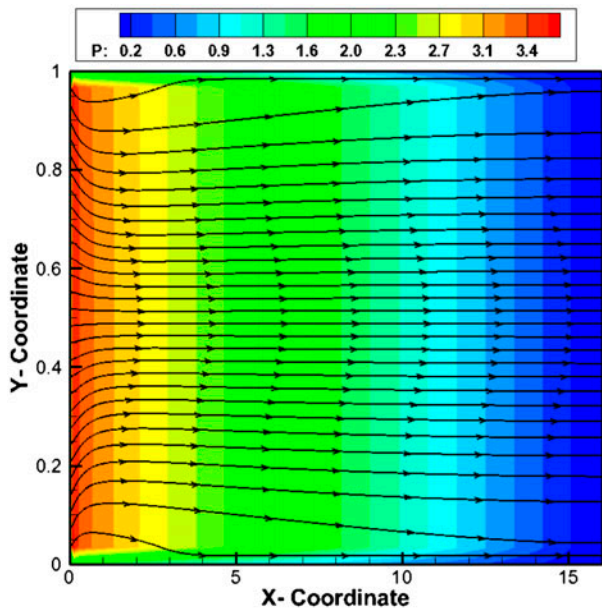


Fig. 8. Streamline and pressure contour in dilute compartment ($Re = 50$).

another iterative loop of the finite difference method to calculate the final value for velocity. So long as ϵ_2 (Eq. (39)) is larger than the acceptable error value, the iterations will continue. At this point, velocity and pressure have been determined for the whole domain, and their values are applied in the mass equations. As long as ϵ_3 and ϵ_4 (Eqs. (40) and (41)) are larger than the acceptable error value, the iterations will continue. Lastly, when the mass equation

is solved, the concentration and potential profile can be determined:

$$\epsilon_1 = \sum_{i=1}^{N_x} \sum_{j=1}^{N_y} |P_{i,j}^{k+1} - P_{i,j}^k| \tag{38}$$

$$\epsilon_2 = \sum_{i=1}^{N_x} \sum_{j=1}^{N_y} |U_{x_{i,j}}^{k+1} - U_{x_{i,j}}^k| + |U_{y_{i,j}}^{k+1} - U_{y_{i,j}}^k| \tag{39}$$

$$\epsilon_3 = \sum_{i=1}^{N_x} \sum_{j=1}^{N_y} |C_{1_{i,j}}^{k+1} - C_{1_{i,j}}^k| \tag{40}$$

$$\epsilon_4 = \sum_{i=1}^{N_x} \sum_{j=1}^{N_y} |C_{2_{i,j}}^{k+1} - C_{2_{i,j}}^k| \tag{41}$$

3. Results and discussion

The model parameters have been calculated using General Electric (GE) membrane type GE-AR908 as an anion removal membrane and GE-CR67 as a cation removal membrane. Table 6 shows the parameters used for the model. All the results are dimensionless quantities.

3.1. Model validation

To assess the accuracy of the developed model, model validation was carried out by comparing the

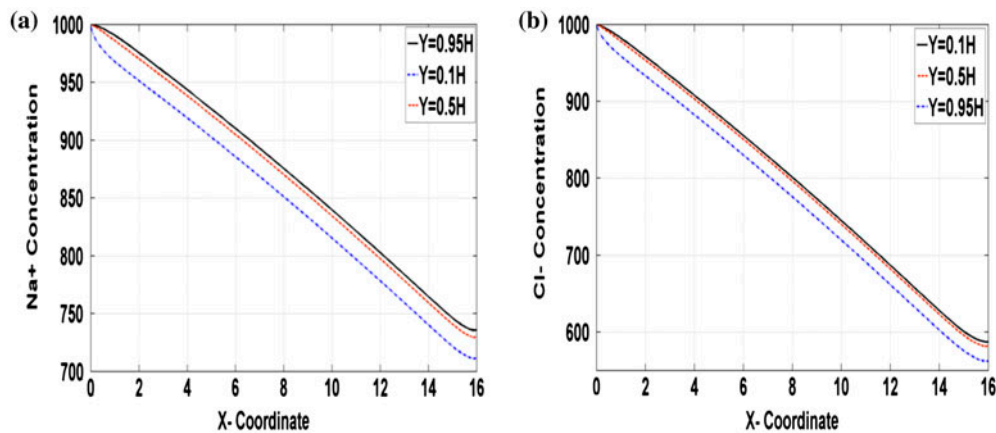


Fig. 9. Concentration distribution (a) for Na^+ and (b) for Cl^- in dilute compartment along the x -axis at constant density ($I = 50$) and constant Re number ($Re = 50$).

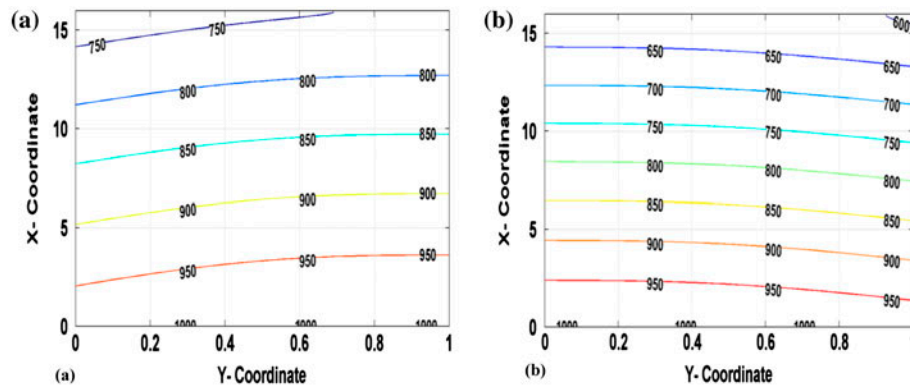


Fig. 10. Concentration contour (a) for Na^+ and (b) for Cl^- in dilute compartment at constant current density ($I = 50$) and constant Re number ($Re = 50$).

developed model with the extended Nernst–Planck, as shown in Eqs. (11) and (17). The results are shown in Fig. 4. As can be seen in this figure, the results from theory and from the developed model align very closely. Notably, a major advantage of the developed model is that it predicts a detailed distribution of concentration and potential drop in both directions by considering all three contributions (migration, diffusion, and convection).

3.2. Fluid flow analysis in dilute chamber

The fluid profiles in Figs. 5 through 8 are simulated by solving the Navier–Stokes equation.

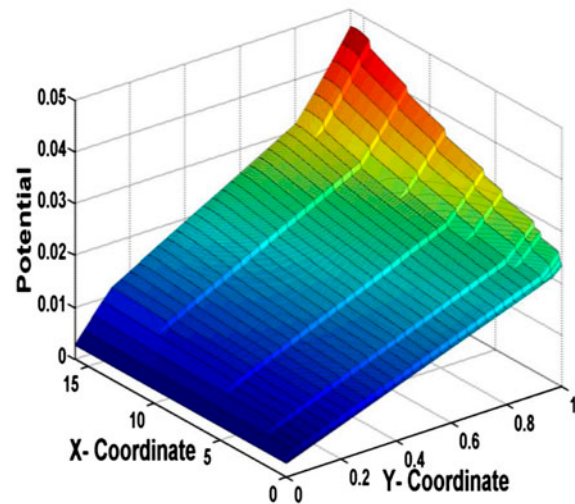


Fig. 12. Potential distribution at constant density ($I = 50$) and constant Re number ($Re = 50$).

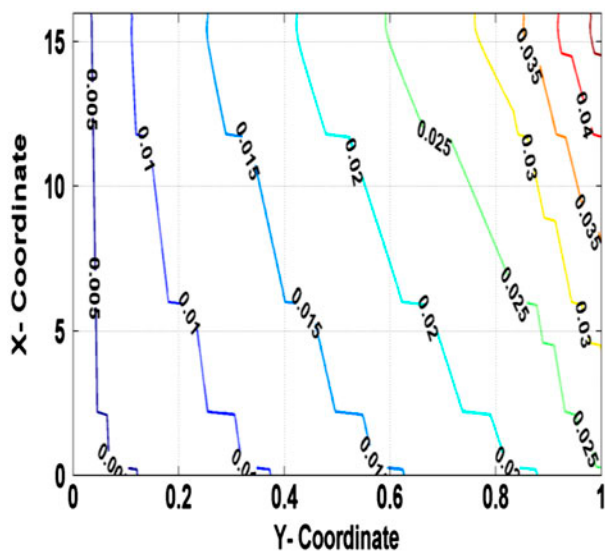


Fig. 11. Potential contour at constant density ($I = 50$) and constant Re number ($Re = 50$).

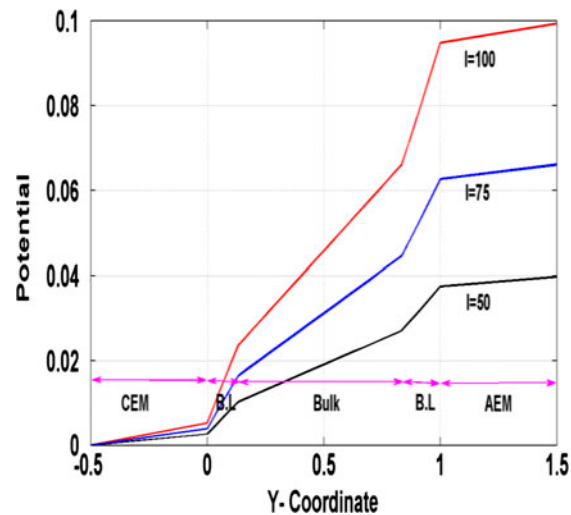


Fig. 13. Potential distribution at different current densities and $Re = 50$.

Fig. 5 shows the momentum and mass transfer boundary layers for $Re = 50$. The thickness of the mass boundary layer on an AEM is larger than that on a CEM because the mobility of chloride ions is higher than that of sodium ions.

Figs. 6 and 7 show the velocity profile along the channel length. As can be seen from Fig. 6, the channel velocity profile before $X = L/16$ is not parabolic because of the short transient time; after $X = L/16$, the parabolicity becomes more apparent as the process continues and the fluid flow in the channel becomes fully developed.

Fig. 8 shows the streamlines and pressure contours in the dilute compartment for $Re = 50$. As can be seen, the pressure decreases along the flow path and also decreases from the center toward the

membrane wall; the streamlines become parallel after a short distance.

3.3. Concentration and potential drop distribution in dilute chamber

Fig. 9 illustrates the concentration distribution for sodium and chloride in the dilute compartment along the x -axis at different distances from the membranes at a constant current density ($I = 50$) and constant Re number ($Re = 50$).

As can be seen from this figure, the concentration distribution for both sodium and chloride ions decreases along the channel. With increasing distance from each membrane surface, separation percentage increases. The reduction in Cl^- concentra-

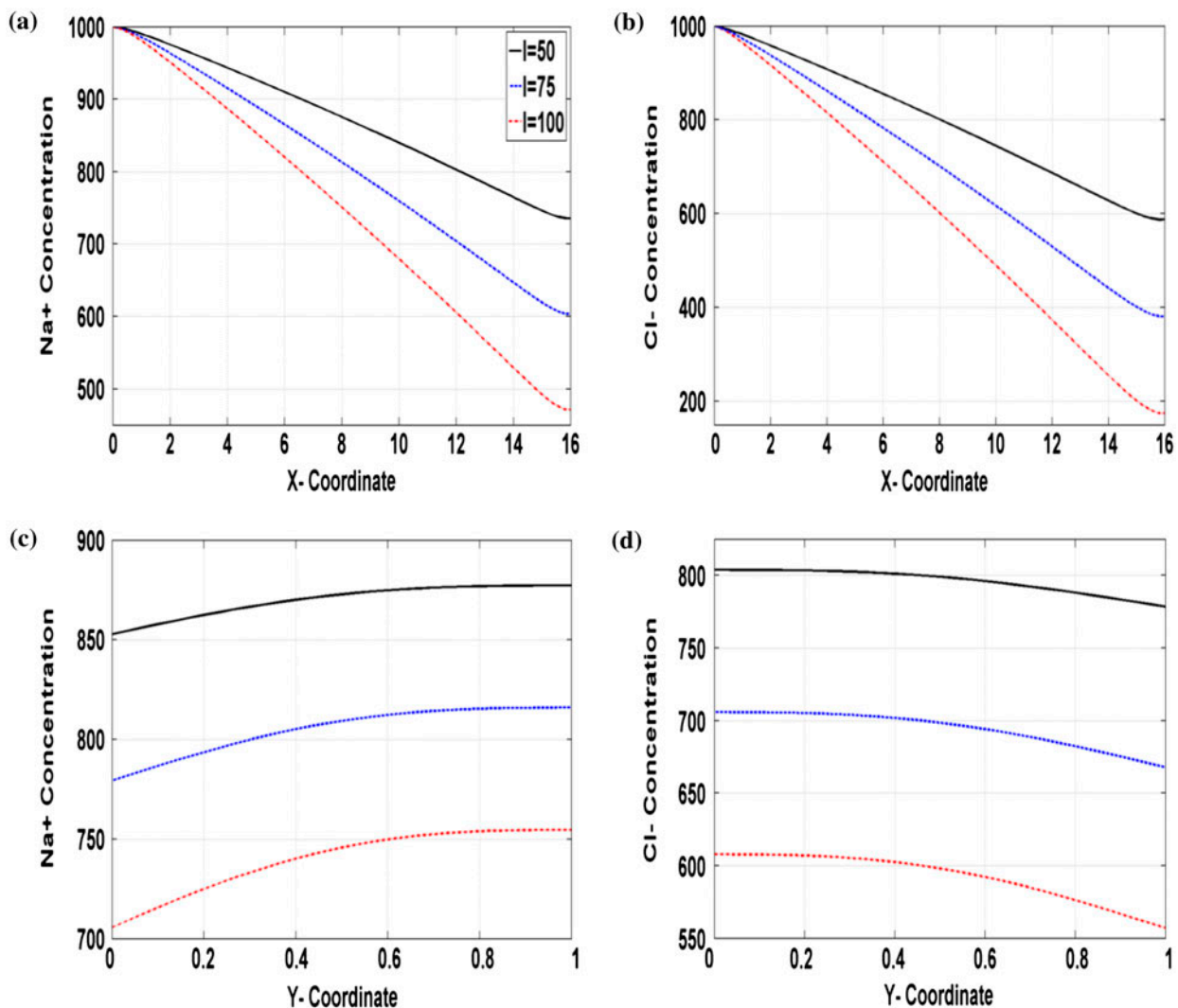


Fig. 14. Concentration distribution in dilute compartment at different current densities and $Re = 50$ (a) for Na^+ along the x -axis, (b) for Cl^- along the x -axis, (c) for Na^+ along the y -axis, and (d) for Cl^- along the y -axis.

tion is more pronounced than the reduction for Na^+ because the mobility for Cl^- is higher than the mobility for Na^+ .

As can be seen from Fig. 9(a), sodium ions' concentration is highest at $Y = 0.95 H$, a point close to the AEM. The reason for this is that sodium ions cannot pass through the AEM. Fig. 9(b) shows that the chloride ion concentration is highest at $Y = 0.1 H$ because chloride flux is zero at the CEM.

Fig. 10 shows the concentration contour (a) for Na^+ and (b) for Cl^- in the dilute compartment at constant current density ($I = 50$) and constant Re number ($Re = 50$).

As can be seen from Fig. 10(a), at a constant distance from the inlet, the concentration of sodium ions will increase with increasing distance from the CEM. This is expected because sodium flux is zero at the AEM. In Fig. 10(b), the opposite trend is shown for chloride.

At a constant distance from each membrane, the concentration of both ions will decrease along the channel length.

Figs. 11 and 12 show the ED system's potential contour and three-dimensional potential distribution, respectively, at constant current density ($I = 50$) and constant Re number ($Re = 50$). As can be seen, in both x - and y -directions, potential increases with increasing distance from the inlet and CEM. The potential gradient in the boundary layer close to the CEM is greater than that close to the AEM.

3.4. Effect of current density on potential drop and ion separation

Fig. 13 shows the potential distribution at different current densities and constant Re numbers ($Re = 50$) along the y -axis at half of the cell length. There are five regions in this figure: AEM, CEM, two boundary layers, and bulk. As can be seen, in each individual current density, the main part of the potential drop occurs in the boundary layers because these regions have higher concentrations of ions than the other regions. With increasing the current density, potential increases. Also, as can be seen, the slope of each region increases with the increase in current density. This means the potential drop also will increase.

Fig. 14 shows concentration distribution in the dilute compartment at constant Re number ($Re = 50$) and different current densities for Na^+ and Cl^- along the x -axis and the y -axis. This figure illustrates the effect of current density on ion concentration distribution at constant Re number. According to Fig. 14, increasing the current density causes an increase in the concentration gradient, and therefore causes higher ion separation (higher separation percent). This occurs because a greater current density means a higher driving force to the system, so ions are forced to move more and transfer across and along the channel.

In terms of how current density affects separation percentage, (separation % = $(C_0 - C)/C_0 \times 100$), the

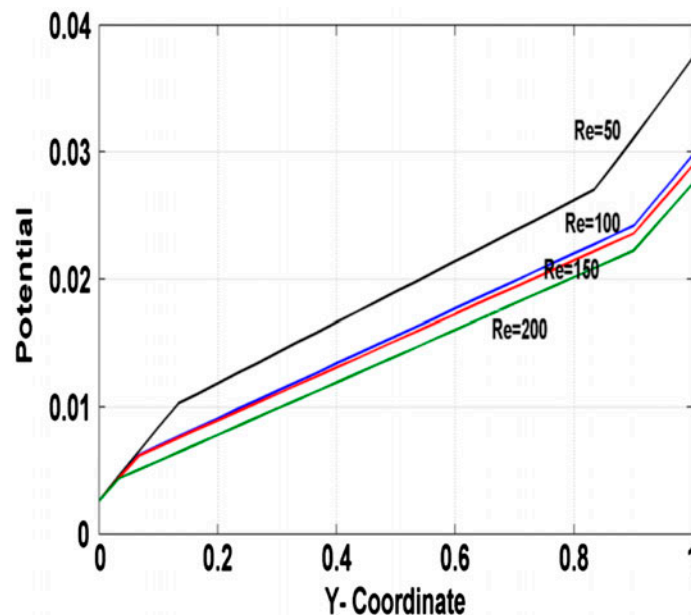


Fig. 15. Potential distribution at different Re numbers and $I = 50$.

developed model predicts that a doubling in current density (50–100 A m⁻²) will roughly double the separation percentage. These predictions are close to the results reported by Shaposhnik et al. [27], who found separation percentage to increase from approximately 50–80% when current density was doubled (10–20 A m⁻²).

3.5. Effect of convection on potential drop and ion separation

Fig. 15 shows the potential distribution for different *Re* numbers along the *y*-axis at half of the cell length. As can be seen, with increases in the *Re* num-

ber, the boundary layer thickness will decrease and the residence time will decrease, causing a decrease in the potential drop.

Fig. 16 illustrates the effect of *Re* number (inlet velocity) on concentration distribution at constant current density (*I* = 50). In theory, by increasing the *Re* number, boundary layer thickness will decrease and mass transfer will increase. The increase in mass transfer is not observed in Fig. 16(a) and (b). However, because the fluid had a shorter contact time with the membrane surface, the ions did not have enough time to diffuse through the membranes. Across the channels, different *Re* numbers did not have a significant effect on ion separation, as shown in Fig. 16(c) and (d).

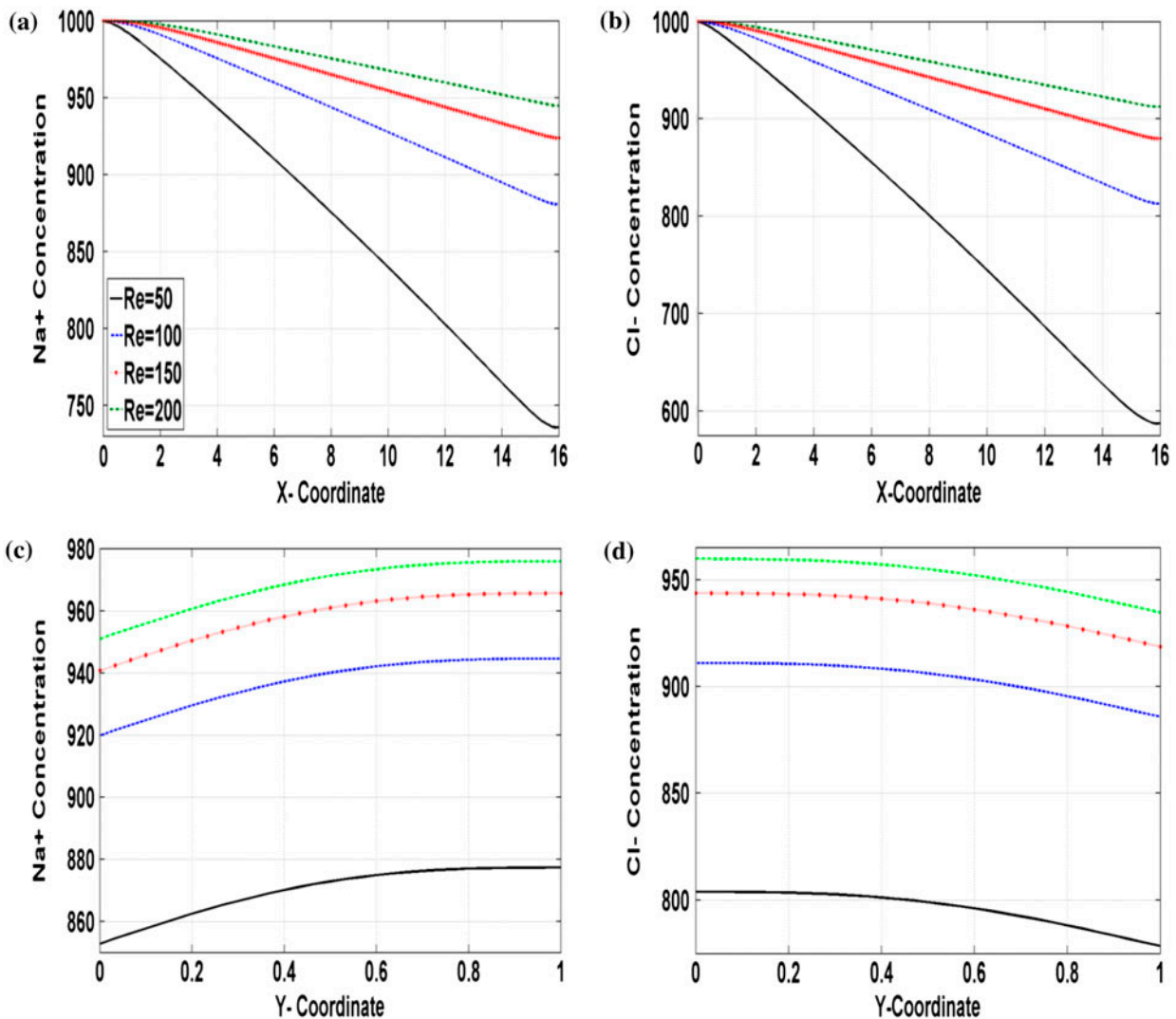


Fig. 16. Concentration distribution in dilute compartment at different *Re* numbers and *I* = 50 (a) for Na⁺ along the *x*-axis, (b) for Cl⁻ along the *x*-axis, (c) for Na⁺ along the *y*-axis, and (d) for Cl⁻ along the *y*-axis.

As can be seen from Fig. 16(a) and (b), when the Re number is decreased (150–50), our model predicts the separation percent to increase about 70%. This finding is broadly consistent with the work of Sadrzadeh et al. [35], who showed that at lower flow rates (i.e. lower Re numbers), the amount of salt separation increases and separation performance increases; the mathematical and experimental results from Sadrzadeh et al. show the separation percent to increase about 60% when the flow rate is decreased to 1/3 (0.6–0.2 mL/s). The difference in the degree of change for predicted separation percent can be attributed to the inclusion of the convection term in our model.

4. Conclusions

This study develops a three-dimensional model that completes previous models by incorporating the factor of convection to predict NaCl mass transport through a rectangular ED cell. The equations used in the model were solved by the finite difference numerical method, using appropriate fluid and mass boundary conditions in the particular control volumes.

In order to verify whether the developed model accurately represents the behavior of ED systems, the model was compared with theory. The results proved to be very consistent with the predictions of theory. The model also expands on the information given by the Nernst–Planck equation, offering information about the distribution of concentration and potential drop in both directions, as compared to the one direction considered in previous studies. This suggests that including the convection term results in a more complete model; therefore, when accuracy is desirable, the convection term should not be neglected.

The ability to calculate concentration distribution in two axes also yielded an interesting finding: regardless of the levels for the Re number and current density, the changes in ionic concentration along the x -axis (flow direction) were greater than the relatively small changes along the y -axis (current direction).

In addition to its theoretical implications, the model has practical use for the design and operation of ED systems: with this model, the user provides input parameters, such as membrane characteristics and system dynamics, and the model then predicts velocity distribution, separation percent, ion concentration distribution, and potential distribution in the dilute chamber.

To further investigate the accuracy of the developed model, future studies could compare its predictions with experimental results.

Acknowledgment

This work is supported by the Office of Naval Research (ONR).

References

- [1] N. Kabay, M. Arda, I. Kurucaovali, E. Ersöz, H. Kahveci, S. Dal, S. Kopuzlu, M. Haner, M. Demircioğlu, M. Yuksel, Effect of feed characteristics on the separation performance of monovalent and divalent salts by electrodialysis, *Desalination* 158 (2003) 95–100.
- [2] N. Kabay, M. Demircioğlu, E. Ersöz, I. Kurucaovali, Removal of calcium and magnesium hardness by electrodialysis, *Desalination* 149 (2002) 343–349.
- [3] L. Greenlee, D. Lawler, B. Freeman, B. Marrot, P. Moulin, Reverse osmosis desalination: Water sources, technology, and today's challenges, *Water Res.* 43 (2009) 2317.
- [4] P.H. Gleick, in: S.H. Schneider (Ed.), *Water Resources in Encyclopedia of Climate and Weather*, 2, University Press, New York, NY, 1996, pp. 817–823.
- [5] W.S. Walker, Improving Recovery in Reverse Osmosis Desalination of Inland Brackish Ground Waters via Electrodialysis, The University of Texas at Austin, August 2010.
- [6] M. Demircioğlu, N. Kabay, E. Ersöz, İ. Kurucaovali, Ç. Şafak, N. Gizli, Cost comparison and efficiency modeling in the electrodialysis of brine, *Desalination* 136 (2001) 317–323.
- [7] R. Valerdi-Perez, M. Lopez-Rodriguez, J.A. Ibáñez-Mengual, Characterizing an electrodialysis reversal pilot plant, *Desalination* 137 (2001) 199–206.
- [8] H. Strathmann, Electrodialysis, a mature technology with a multitude of new applications, *Desalination* 264 (2010) 268.
- [9] L. Karimi, A. Ghassemi, Effects of operating conditions on ion removal from brackish water using a pilot-scale electrodialysis reversal system, *Desalin. Water Treat.* (In Press) (2015), doi: [10.1080/19443994.2015.1024748](https://doi.org/10.1080/19443994.2015.1024748).
- [10] K. Mitko, M. Turek, Concentration distribution along the electrodialyzer, *Desalination* 341 (2014) 94–100.
- [11] V.M. Volgin, A.D. Davydov, Ionic transport through ion-exchange and bipolar membranes, *J. Membr. Sci.* 259 (2005) 110–121.
- [12] V.M. Volgin, A.D. Davydov, Numerical modeling of non-steady-state ion transfer in electrochemical systems with allowance for migration, *Russ. J. Electrochem.* 37(11) (2001) 1197–1205.
- [13] N.P. Gnusin, Mathematical model of electro-diffusion transfer through a diffusion layer–heterogeneous ion-exchange membrane system, *Russ. J. Electrochem.* 39 (10) (2003) 1053–1057.
- [14] N.P. Gnusin, Modeling of mass electron transfer in an electrodialysis cell, *Theor. Found. Chem. Eng.* 38(3) (2004) 296–300.
- [15] V.M. Volgin, O.V. Volgina, A.D. Davydov, Numerical modeling of steady-state ion transfer in electrochemical systems with allowance for migration, *Russ. J. Electrochem.* 38(10) (2002) 1059–1067.
- [16] M. Fidaleo, M. Moresi, Optimal strategy to model the electrodialytic recovery of a strong electrolyte, *J. Membr. Sci.* 260 (2005) 90–111.

- [17] V. Nikonenko, V. Zabolotsky, C. Larchet, B. Auclair, G. Pourcelly, Mathematical description of ion transport in membrane systems, *Desalination* 147 (2002) 369–374.
- [18] V.I. Zabolotsky, J.A. Manzanares, V.V. Nikonenko, K.A. Lebedev, E.G. Lovtsov, Space charge effect on competitive ion transport through ion-exchange membranes, *Desalination* 147 (2002) 367–392.
- [19] A.A. Moya, Steady-state and transient electrical properties of ion-exchange membrane systems in asymmetric arrangements, *Russ. J. Electrochem.* 48(7) (2012) 738–745.
- [20] A. Pismenskiy, V. Nikonenko, M. Urtenov, G. Pourcelly, Mathematical modelling of gravitational convection in electro dialysis processes, *Desalination* 192 (2006) 374–379.
- [21] Y. Kim, W.S. Walker, D.F. Lawler, Electro dialysis with spacers: Effects of variation and correlation of boundary layer thickness, *Desalination* 247 (2011) 54–63.
- [22] N.P. Gnusin, Mathematical model of electro-diffusion transfer through three-layer membrane system: Diffusion layer–ion-exchange membrane–diffusion layer, *Russ. J. Electrochem.* 45(10) (2009) 1149–1155.
- [23] M. Fidaleo, M. Moresi, A. Cammaroto, N. Ladrage, R. Nardi, Modelling of soy sauce desalting by electro dialysis, *Food Bioprocess Technol.* 16 (2012) 1–15.
- [24] V. Nikonenko, K. Lebedev, J. Manzanares, G. Pourcelly, Modelling the transport of carbonic acid anions through anion-exchange membranes, *Electrochim. Acta* 48 (2003) 3639–3650.
- [25] F.S. Rohman, N. Aziz, Mathematical model of ion transport in electro dialysis process, *Bull. Chem. React. Eng. Catal.* 3(1–3) (2008) 3–8.
- [26] M. Fidaleo, M. Moresi, Electro dialytic desalting of model concentrated NaCl brines as such or enriched with a non-electrolyte osmotic component, *J. Membr. Sci.* 367 (2011) 220–232.
- [27] V.A. Shaposhnik, V.A. Kuzminykh, O.V. Grigorochuk, V.I. Vasileva, Analytical model of laminar flow electro dialysis with ion-exchange membranes, *J. Membr. Sci.* 133 (1997) 27–37.
- [28] V.A. Shaposhnik, O.V. Grigorochuk, E.N. Korzhov, V.I. Vasileva, V.Y. Klimov, The effect of ion-conducting spacers on mass transfer—Numerical analysis and concentration field visualization by means of laser interferometry, *J. Membr. Sci.* 139 (1998) 85–96.
- [29] A.A. Sonin, R.F. Probst, A hydrodynamic theory of desalination by electro dialysis, *Desalination* 5 (1968) 293–329.
- [30] N.P. Gnusin, O.A. Demina, N.P. Berezina, N.A. Kononenko, Modeling of mass electro transfer in terms of the transport and structural properties of ion-exchange membranes, *Theor. Found. Chem. Eng.* 38(4) (2004) 394–398.
- [31] V.A. Shaposhnik, O.V. Grigorochuk, Mathematical model of electro dialysis with ion-exchange membrane and insert spacers, *Russ. J. Electrochem.* 46(10) (2010) 1182–1188.
- [32] Y. Kim, W.S. Walker, D.F. Lawler, Competitive separation of di- vs. mono-valent cations in electro dialysis: Effects of the boundary layer properties, *Water Res.* 46 (2012) 2042–2056.
- [33] F.G. Helfferich, *Ion Exchange*, McGraw-Hill Book Company Inc, New York, NY, 1962.
- [34] P. Dutta, A. Beskok, Analytical solution of combined electroosmotic/pressure driven flows in two-dimensional straight channels: Finite Debye layer effects, *Anal. Chem.* 73 (2001) 1979–1986.
- [35] M. Sadrzadeh, T. Mohammadi, J. Ivakpour, N. Kasiri, Separation of lead ions from wastewater using electro dialysis: Comparing mathematical and neural network modeling, *Chem. Eng. J.* 144 (2008) 431–441.